The Effect of Weave Orientation on the BRDF of Tarp Samples

Georgi T. Georgiev[a], James J. Butler[b]

[a]Science Systems and Applications, Inc., Lanham, MD 20706, e-mail: gtg@spectral2.gsfc.nasa.gov
[b]NASA Goddard Space Flight Center, Code 920.1, Greenbelt, MD 20771

ABSTRACT

The results of bi-directional reflectance distribution function (BRDF) measurements of four tarp samples obtained from NASA's Stennis Space Center (SSC) are presented. The measurements were performed in the Diffuser Calibration Facility (DCaF) at NASA's Goddard Space Flight Center (GSFC). The samples are of similar material structure but different reflectance. The experimental data were obtained with a Xe arc lamp/monochromator light source as well as laser light sources in the ultraviolet, visible, and near infrared spectral regions. The BRDF data were recorded at four incident zenith angles and at five incident azimuth angles. The dependence of the measured BRDF on weave orientation was analyzed and presented. 8 degree directional/hemispherical reflectance data were also measured for each tarp sample, and those results are also reported. All results are NIST traceable through calibrated standard plates. The specular and diffuse scatter data obtained from these studies are used by NASA's SSC in their field-based, vicarious calibration of satellite and airborne remote sensing instruments.

Keywords: Optical scattering, BRDF, Hemispherical reflectance, Reflectance spectroscopy, Polarization optics.

1. INTRODUCTION

We are presenting the results of BRDF and 8° directional/hemispherical reflectance measurements performed in the Diffuser Calibration Facility (DCaF) at NASA's Goddard Space Flight Center (GSFC) on tarp samples obtained from NASA's SSC. The facility scatterometer[1], located in a class 10,000 laminar flow cleanroom, is a fully automated instrument capable of measuring the BRDF of a wide range of sample types in the spectral range from 230nm to 900nm. The scatterometer can perform in-plane and out-of-plane BRDF measurements with typical measurement uncertainty of less than 1.0% (k = 1). Recently, the scatterometer measurement capabilities were expanded with a new integrating sphere designed and built for 8° directional/hemispherical reflectance measurements in the UV, VIS and NIR spectral range. The uncertainty of the 8° directional/hemispherical reflectance measurements is less than 1.0% (k = 1) for the setup used. The scatterometer is regularly calibrated, and the results presented are traceable to measurements made on the National Institute of Standards and Technology's (NIST's) Special Tri-function Automated Reference Reflectometer (STARR)[2].

The reported data are intended to more completely describe the optical scatter characteristics of tarp samples and the effect of weave orientation on their BRDF when the tarps are used in the vicarious calibration of satellite and airborne remote sensing instruments. The tarp samples are witness pieces from larger field-deployed tarps. The dimensions of the samples are 10 x 10.5 cm, cut along the weft (tight) threads. The tarps are of similar material structure but with values of 8° directional/hemispherical reflectance from 70% to 4%. The samples exhibit a wide range of BRDF values depending on angle of incidence and scatter. Their surface can be modeled as a highly regular wave-like structure of a man-made material. We are presenting BRDF and 8° directional/hemispherical reflectance data measured at 485, 550, 633 and 800 nm. The results show strong dependence in BRDF on the weave orientation relative to the incident beam direction. The magnitude of the difference varies and can be as high as 17% depending on the incident and scattered light angles. The presented results are of practical interest for NASA's SSC vicarious calibrations. The high

quality of the data is supported by the fact the measurements were done in a clean room calibration facility and the results are NIST traceable.

2. BACKGROUND

As shown in Fig. 1, the BRDF is usually referred to as the ratio of the scattered radiance L_s scattered by a surface into the direction (θ_s, ϕ_s) to the collimated irradiance E_i incident on a unit area of the surface[3]:

$$BRDF = \frac{L_s(\theta_i, \phi_i, \theta_s, \phi_s, \lambda)}{E_i(\theta_i, \phi_i, \lambda)}, \quad (1)$$

where θ is the zenith angle, ϕ is the azimuthal angle, the subscripts *i* and *s* are for the incident and scattered (or detector) directions respectively, and λ is the wavelength. In practice, we usually present BRDF in terms of the incident power, scattered power and the geometry of the reflected scatter. It is equal to the scattered power per unit solid angle normalized by the incident power and the cosine of the detector view angle[4]:

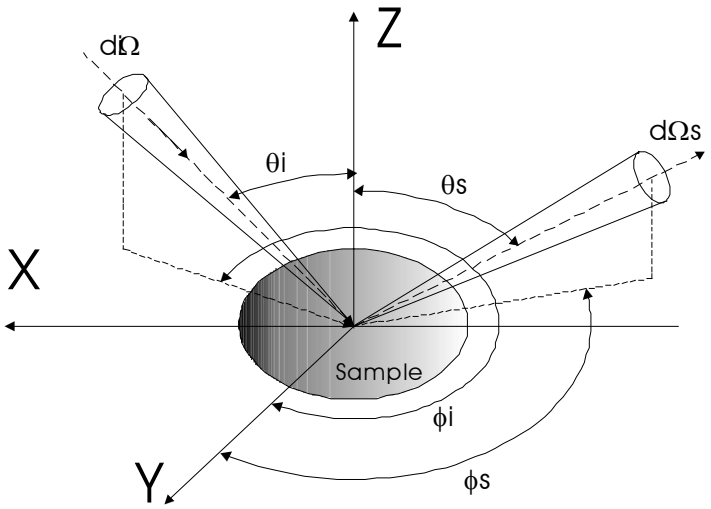

Fig.1 Defining the BRDF in terms of usually adopted symbols

$$BRDF = \frac{P_s / \Omega}{P_i \cos\theta_s}, \quad (2)$$

where P_s is the scatter power, Ω is the solid angle determined by the detector aperture, *A*, and the radius from the sample to the detector, *R*, or $\Omega = A/R^2$, P_i is the incident power, and θ_s is the detector zenith angle.

The 1.0% uncertainty specification of the measurement depends on several instrument variables[1]. The uncertainty in a BRDF measurement, Δ_{BRDF}, evaluated and expressed in accordance with NIST guidelines[5] is presented by

$$(\Delta_{BRDF})^2 = 2(\Delta_{NS})^2 + 2(\Delta_{LIN})^2 + (\Delta_{SLD})^2 + (\Delta_{\theta s}\tan(\theta_s))^2, \quad (3)$$

where Δ_{NS} is the noise to signal ratio, Δ_{LIN} is the non-linearity of the electronics, Δ_{SLD} is the error of the receiver view angle, $\Delta_{\theta s}$ is the error of the total scatter angle, and θ_s is the error of the receiver scatter angle. The error of the receiver view angle, Δ_{SLD}, can be further expressed by

$$(\Delta_{SLD})^2 = (2\Delta_{RM})^2 + (2\Delta_{RZ})^2 + (2\Delta_{RA})^2, \quad (4)$$

where Δ_{RM} is the error of the receiver arm radius due to the goniometer, Δ_{RZ} is the error of the receiver arm radius due to sample Z direction misalignment, and Δ_{RA} is the error of the receiver aperture radius. The total scatter angle error, $\Delta_{\theta s}$, can be expressed by

$$(\Delta_{\theta s})^2 = (\Delta_{\theta M})^2 + (\Delta_{\theta Z})^2 + (\Delta_{\theta T})^2, \quad (5)$$

where $\Delta_{\theta M}$ is the error of the scatter angle due to the goniometer, $\Delta_{\theta Z}$ is the error due to sample Z direction misalignment, and $\Delta_{\theta T}$ is the sample tilt error.

The 8° directional/hemispherical reflectance integrating sphere collects and spatially integrates the scattered optical radiation. The sphere interior is Spectralon with typical reflectance of 94% to 99% from the UV to the NIR. The sphere was designed with several ports to accommodate the sample, the detector, and the entry of the incident light. A fourth port is a spare and is typically closed using a Spectralon plug. The total port area is less than 5% of the total surface area of the sphere. It is important to have the radiation balance inside the sphere established after as few internal reflections as possible. The light intensity incident on the detector should correspond to the average light intensity inside the sphere. An interior baffle is employed to block the detector viewing light reflected directly from the sample.

3. EXPERIMENTS AND DISCUSSION

Bidirectional reflectance distribution function: setup and measurements

We used the DCaF scatterometer to measure each sample's BRDF at different source and detector angular configurations. The calibration items were mounted in a holder on the sample stage so to be both aligned with the axes of rotation. The fiducial marks of the samples were fixed in front of the goniometer. The angular convention is shown in Fig.1. The detector field-of-view was centered on the calibration items for all measurements. The detector field-of-view was underfilled by the incident beam, which had a spectral bandwidth of 12 nm. The measurements were performed at source zenith angles of 0°, 10°, 20°, and 30° and at source azimuth angles of 0° and 90° for each source zenith angle. The detector angles were –detector zenith: 0°, 10°, 20°, 30°, 40°, 50° and 60°; detector azimuth: 0°, 45°, 90°, 135° and 180° for each detector zenith angle. The light source was a 75 W Xenon lamp coupled to a Chromex 0.25m monochromator. The monochromatic light beam was mechanically chopped. Scattered light was detected using an ultraviolet enhanced silicon photodiode with output fed to a computer-controlled lock-in amplifier. For better characterization of the material scatter, data were collected at 485, 550, 633 and 800 nm for each source-detector angle combination. All measurements were made for polarizations of the illumination beam both parallel and perpendicular to the plane of incidence and the unpolarized scatter is reported in this paper. The scatterometer was calibrated using NIST calibrated Spectralon samples. The tarp samples surface structure is shown in Figs.2.a,b and the sample positioned on the sample stage is shown in Fig.3.

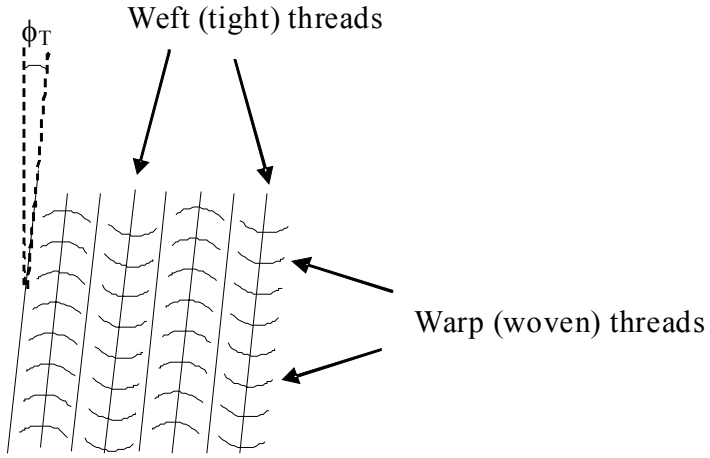

Fig.2.a: Tarp surface structure

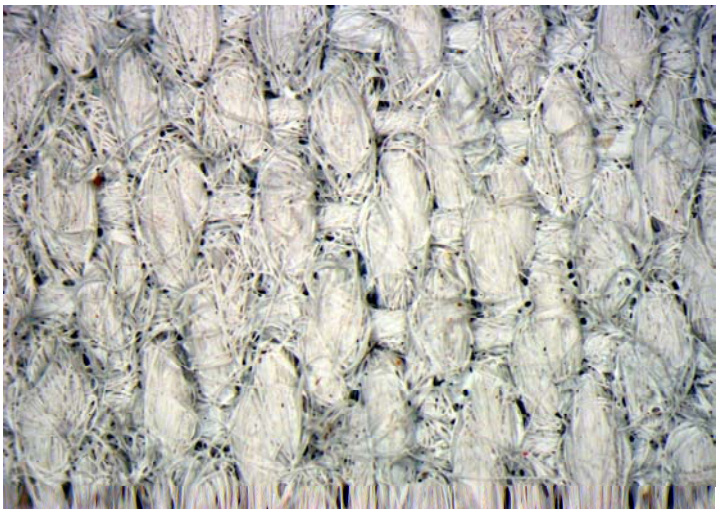

Fig.2.b: Microscopic image of Tarp #1

BRDF at normal incidence

Fig. 4 shows the BRDF of sample 1, acquired at 0° incidence and at 485 nm for 5 different detector azimuth positions. The detector zenith angles vary from 10° to 60° in 10° steps. It is well evident the BRDF decreases with increasing detector zenith angle for all detector azimuth positions. Our BRDF measurements at 550, 633 and 800 nm of samples #2, #3 and #4 show the same tendency. On the other hand the BRDF depends on the detector azimuth angle for all detector zenith positions. We recorded the highest values at 0° and 180° azimuth. At these angles the detector is scanning into the plane defined by the sample weft threads as it is shown in Fig.2.a. The BRDF difference is small - less than 0.5% and is due to non-uniformity of the sample surface structure in forward and backward scatter. The BRDF decreases for 45° and 135° detector azimuth as the detector scanning plane is rotated 45° relative to the sample weft threads at these measurements. The difference is an average of 1.5% for all samples and is attributed again to the sample's surface structure. The lowest BRDF was measured at 90° detector azimuth, in accordance with our expectations that the detector scanning plane is now perpendicular to the weft threads and the tarp bumps are covering part of the surface (i.e. the shadow effect). The average BRDF measured at 90° detector azimuth is 3% lower than the average BRDF measured at detector azimuths of 45° and 135° and it is 6% lower than the average BRDF measured at detector azimuths of 0° and 180°. These results completely describe the BRDF of the samples under normal illumination and as a function of detector azimuth angle.

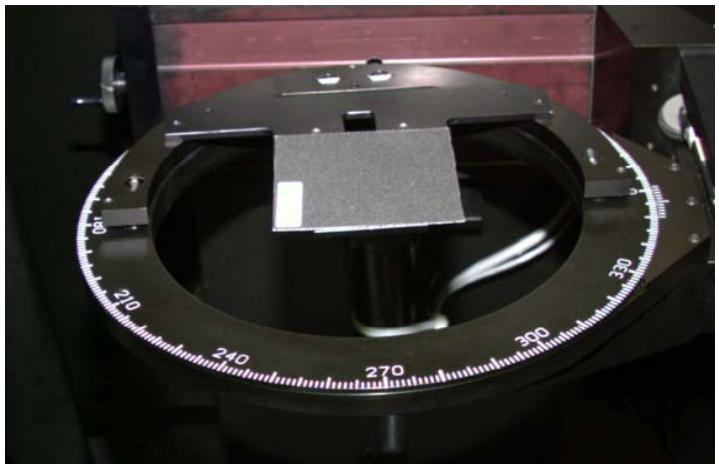

Fig.3: Tarp on the stage, weft threads rotated 4 deg CCW

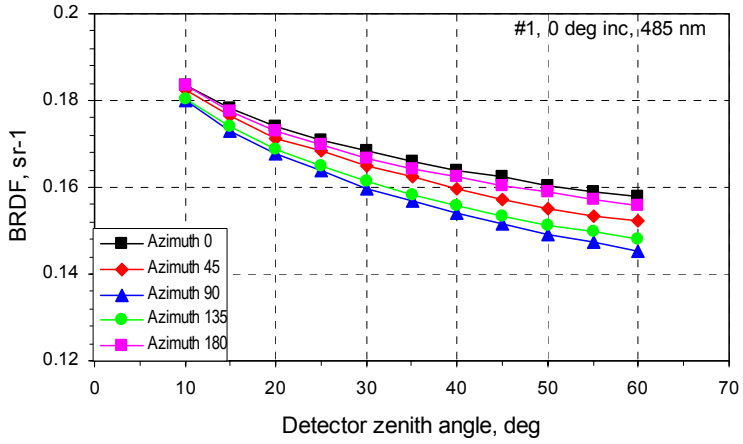

Fig.4: BRDF at normal incidence, 485 nm, sample #1

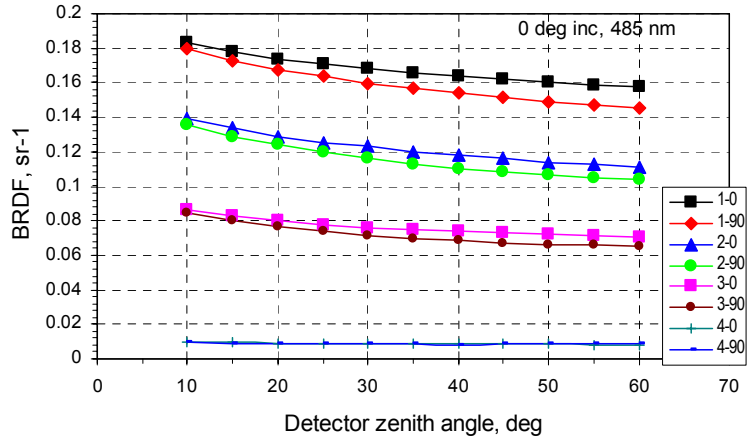

Fig.5: Normal incidence, 0 and 90 deg detector azimuth, 485 nm, samples 1 to 4

The BRDF of the 4 tarp samples measured at normal incidence and at a wavelength of 485 nm is shown in Fig.5 for detector azimuth angles of 0° and 90°. It is evident the slopes of all curves for each sample remain the same at each detector azimuth angle. The BRDF of samples 2, 3 and 4 can be derived from the BRDF of sample 1 with the following correction coefficients: 1 to 2: 0.73; 1 to 3: 0.45; 1 to 4: 0.05, as the coefficients are the same for both 0° and 90° detector azimuth angles. In

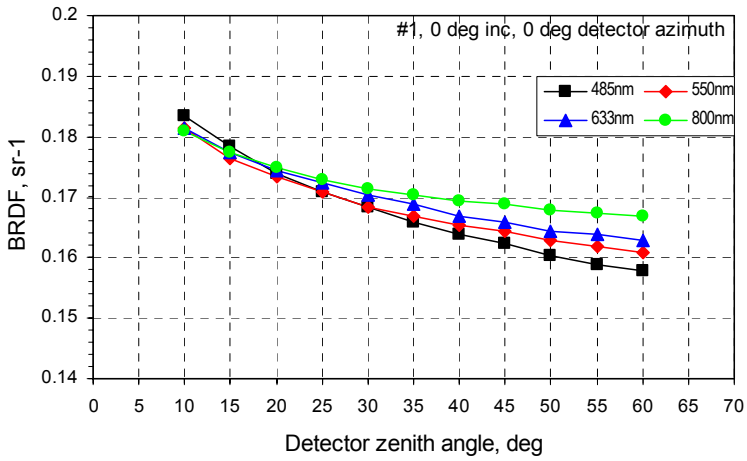

Fig.6: BRDF at 485, 550, 633 and 800 nm; sample #1

the following discussions, we will refer only to sample 1 as there are not substantial calibration differences between all samples except the absolute reflectance of the samples.

The dependence of BRDF on the detector zenith angle at normal incidence and at wavelengths of 485, 550, 633 and 800 nm is given in Fig.6 for sample 1. The BRDF at different wavelengths is defined by (i) the spectrum of the sample's material and (ii) by the detector coordinates. For detector zenith angles bigger than 20°, the spatial reflected light distribution is the prevalent factor; for angles less than 20°, the influence of the material spectral properties is well presented. The BRDF at shorter wavelengths is a slightly higher at smaller scatter elevation angles, while the BRDF at longer wavelengths is significantly higher at larger angles and at longer wavelengths.

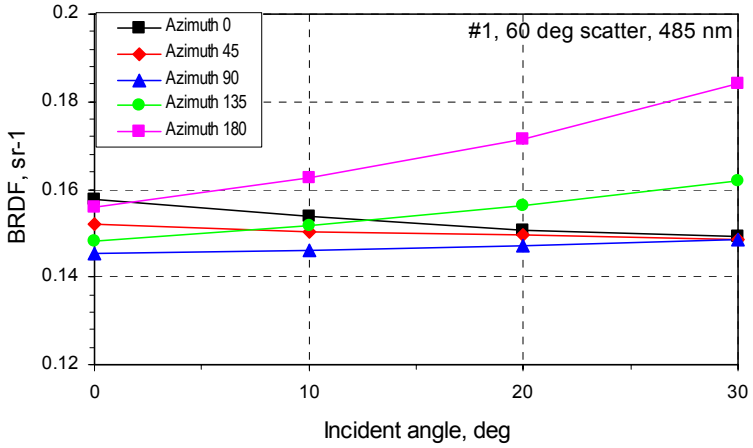

Fig.7: BRDF at 60 deg detector zenith angle, 485 nm, sample #1

BRDF at non-normal angles of incidence

BRDF measured at non-normal incident angles usually is quite different than that measured at normal incidence. In the case of well defined spectrally flat surfaces, such as Spectralon, the BRDF can be accurately modeled and predicted. In the case of complex surfaces such as tarps or fabrics, the experimentally obtained BRDF is of primary importance. Fig.7 shows the dependence of BRDF on the source zenith angle at 60° detector zenith angle and 485 nm for 5 different detector azimuth positions. The BRDF decreases up to 6% and 3% with increasing source zenith angle and detector azimuth angles of 0° and 45°, respectively. The BRDF increases from 3% to 16% with increasing source zenith angle at detector azimuth angles of 90°, 135° and 180°. The differences between BRDF measured at 10° and 30° source zenith angles and at detector azimuth angles of 0°, 45°, 90°, 135° and 180° and detector zenith angles of 10°, 20°, 40° and 60° are shown in Table 1.

Table 1: BRDF difference between 10° and 30° incident angles

Detector zenith angle, deg	Detector azimuth angle, deg				
	0	45	90	135	180
10	-15.55%	-13.50%	-9.16%	-5.56%	-5.52%
20	-12.05%	-8.62%	-3.71%	2.60%	7.54%
40	-9.05%	-5.34%	0.32%	7.76%	17.02%
60	-5.76%	-2.35%	2.35%	8.41%	15.33%

BRDF data measured at 485 nm are plotted in Figs.8.a,b for 10° and 30° source zenith angles. The slopes of the measured curves are the same for both angles for the 0° detector azimuth curves. It is again the same for the 90° detector azimuth curves. There are detectible, differences between the 0° and 90° detector azimuth curves at each point and for each

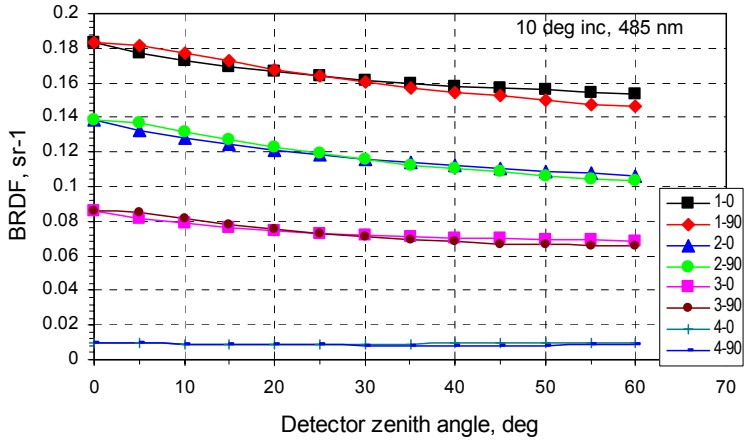

Fig.8.a: 10 deg incidence, 0 and 90 deg detector azimuth, 485 nm, samples 1 to 4

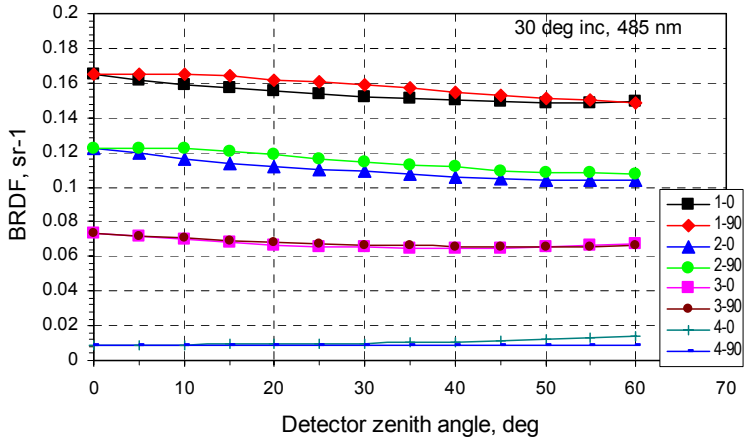

Fig.8.b: 30 deg incidence, 0 and 90 deg detector azimuth, 485 nm, samples 1 to 4

sample. Numerically expressed, that difference is less than 2% for sample 1, 4% for sample 2, 1% for sample 3 at a 30° source zenith angle. The surface structure of the tarp sample shows a different BRDF behavior at 10° source zenith angle. The BRDF below 25° detector zenith angle and at 0° detector azimuth angle is higher than at 90° detector azimuth. Oppositely, at detector zenith angles higher than 25°, the BRDF at 0° detector azimuth angle is higher than that at 90° detector azimuth. The slopes of the curves are again the same comparing the respective sample – detector azimuth pairs.

We also compared the BRDF dependence on detector zenith angle at wavelengths of 485, 550, 633 and 800 nm testing tarp sample 1 at a source zenith angle of 10° and a detector azimuth angle of 0°. Although not as prominent as at normal incidence, the BRDF at shorter wavelengths is slightly higher measured at 0° detector zenith angle and significantly higher for the longer wavelengths at larger detector zenith angles (Fig.9).

8° directional/hemispherical measurement

The 8° directional/hemispherical reflectance of all the tarp samples was measured with HeNe laser at 632.8 nm. The only hardware difference from the experimental setup described in the previous section is the use of an 8° directional/hemispherical integrating sphere mounted above the scatterometer sample stage. This integrating sphere is shown in Fig 10. The silicon photodiode detector was fixed to one port of the sphere. The dependence of the hemispherical reflectance versus receiver power is fitted using a third-degree polynomial regression:

$$R(P) = A + BP - CP^2 + DP^3 \qquad (6)$$

The coefficients of the polynomial can be calculated by fitting the receiver power measured using a set of 7 gray Spectralon standard plates with known 8° directional/hemispherical reflectance. With the setup described above, the power was measured at each wavelength of interest for each standard plate and the coefficients were calculated using a MathCAD 3rd degree

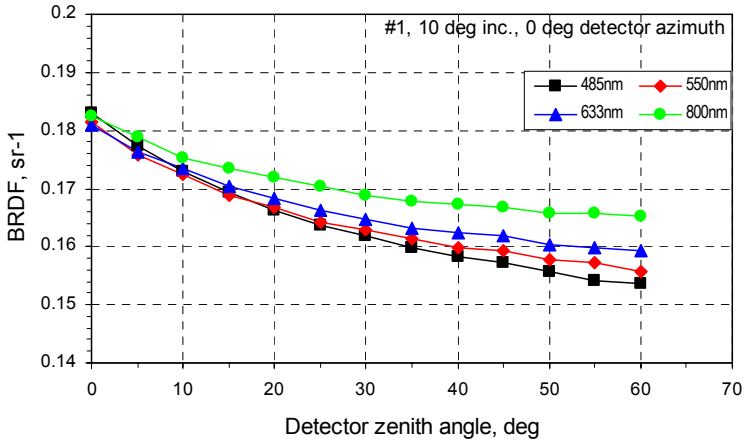

Fig.9: BRDF at 485, 550, 633, 800 nm; sample #1

polynomial fitting procedure. To verify the proposed procedure the distribution of the difference between the Labsphere measured and our measured 8° directional/hemispherical reflectance values of the Spectralon samples of nominal reflectance 5%, 10%, 20%, 40%, 60%, 80% and 99% are shown in Fig. 11. The measured 8° directional/hemispherical reflectance data for each sample are given in Table 2.

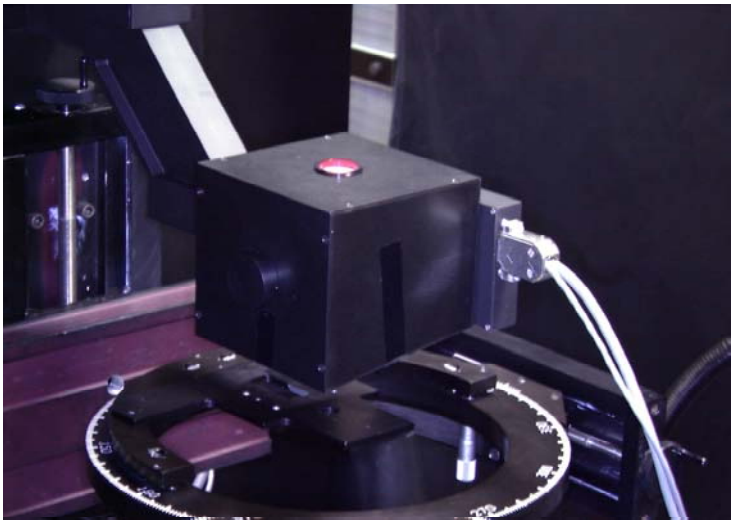

Fig.10: 8° directional/hemispherical reflectance integrating sphere.

CONCLUSIONS

The BRDF and 8° directional/hemispherical reflectance of four tarp samples were measured using the scatterometer located in NASA's GSFC DCaF. A monochromator-based light source in the UV, VIS and NIR spectral regions was used in these measurements. In-plane and out-of-plane geometries were employed in the BRDF measurements at a number of incident source angles and over a range of detector scatter angles. The experimental data show the BRDF dependence on weave orientation of the samples is well defined for both normal and non-normal incident light. BRDF differences vary and can approach 17% for non-normal illumination and can approach 6% for normal illumination. The weave orientation does not show angular differences in the BRDF of the different samples. Any differences can be attributed to the different sample reflectances. Non-normal incident illumination introduces an additional dependence of BRDF on weave orientation. The difference is small but contributes to each sample's BRDF characterization. There is also a spectral dependence of the weave orientation on BRDF which is apparent at lower detector zenith angles over the spectral range from 485 to 800 nm for both normal and non-normal incident light. The 8° directional/hemispherical reflectance data support and complement the BRDF measurements. The BRDF data obtained from these studies are important for future NASA SSC vicarious calibrations through analysis of the BRDF dependence on weave orientation. The BRDF characterization of tarp samples as shown in this paper can be successfully extended to other structured

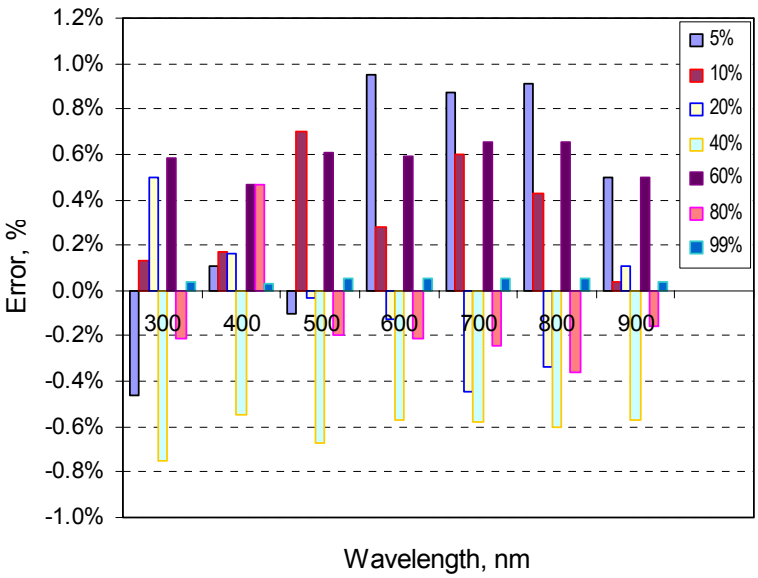

Fig.11: Difference between standard and measured values of 7 Spectralon

Table 2: 8° directional/hemispherical reflectance

Sample	Hemispherical Reflectance
1	67.34%
2	49.65%
3	31.93%
4	4.35%

surface fabric samples. The reported data were measured in a clean room calibration facility; and the results presented are NIST traceable trough calibrated standards.

ACKNOWLEDGEMENTS

The authors would like to thank Mary Pagnutti and Bob Ryan of NASA's Stennis Space Center for making the tarp samples available to us for measurement.

REFERENCES

1. T.F. Schiff, M.W. Knighton, D.J. Wilson, F.M. Cady, J.C. Stover, and J.J. Butler, "A Design Review of a High Accuracy UV to Near Infrared Scatterometer", Proc. SPIE, 1995, 121-130 (1993).

2. J.R. Proctor and P.Y. Barnes, "NIST High accuracy reference reflectometer - spectrophotometer", J. Res. Nat. Inst. Stand. Technol., 101, 619-627, (1996).

3. F.E. Nicodemus, J.C. Richmond, J.J. Hsia, I.W. Ginsburg, and T. Limperis, "Geometrical considerations and nomenclature for reflectance", National Bureau of Standards, NBS monograph 160, Oct. 1977

4. J.C. Stover, "Optical scattering: measurement and analysis", SPIE Press, Bellingham, Washington, 1995

5. B.N. Taylor and C. E. Kuyatt, "A Guidelines for Evaluating and Expressing the Uncertainty of NIST Measurement Results", NIST Technical Note 1297, U.S. Department of Commerce, National Institute of Standards and Technology, Sep. 1997.